ACS APPLIED MATERIALS & INTERFACES

Research Article

www.acsami.org

Strong Improvements of Localized Surface Plasmon Resonance Sensitivity by Using Au/Ag Bimetallic Nanostructures Modified with Polydopamine Films

Kun Jia,[†] Mohammad Y. Khaywah,[†] Yugang Li,[‡] Jean L. Bijeon,[†] Pierre M. Adam,[†] Régis Déturche,[†] Bruno Guelorget,[‡] Manuel François,[‡] Guy Louarn,[§] and Rodica E. Ionescu*[,†]

[†]Laboratoire de Nanotechnologie et d'Instrumentation Optique and [‡]Laboratoire des Systèmes Mécaniques et d'Ingénierie Simultanée, UMR-STMR CNRS 6279, Institute Charles Delaunay, Université de Technologie de Troyes, 12 Rue Marie Curie CS 42060, 10004 Troyes Cedex, France

[§]Laboratoire de Physique des Matériaux et Nanostructures, UMR 6502, Institut des Matériaux Jean Rouxel, 2 Rue de la Houssinière BP 32229, 44322 Nantes Cedex 03, France

Supporting Information

ABSTRACT: In the present work, the standard monometallic localized surface plasmon resonance (LSPR) biosensing sensitivity is highly improved when using a new system based on glass substrates modified with high-temperature annealed gold/silver bimetallic nanoparticles (Au/Ag bimetallic NPs) coated with polydopamine films before biomolecule specific immobilization. Thus, different zones of bimetallic NPs are spatially created onto a glass support thanks to a commercial transmission electron microscopy (TEM) grid marker in combination with two sequential evaporations of continuous films of gold (4 nm) and silver (2 nm) and followed by annealing at 500 °C for 8 h. By using the scanning electron microscopy (SEM), it is found that annealed Au/Ag bimetallic NPs have uniform size and shape distribution that exhibited a sharper well-defined LSPR resonant peak when compared with that of monometallic Au NPs and thereby contributing to an improved sensitivity in LSPR biosensor application. The controlled micropatterns consisting of bimetallic particles are used in the construction of LSPR biochips for high-throughput detection of different concentrations of a model antigen named bovine serum albumin (BSA) on a single glass sample, with a lower limit of detection of 0.01 ng/mL under the optimized conditions.

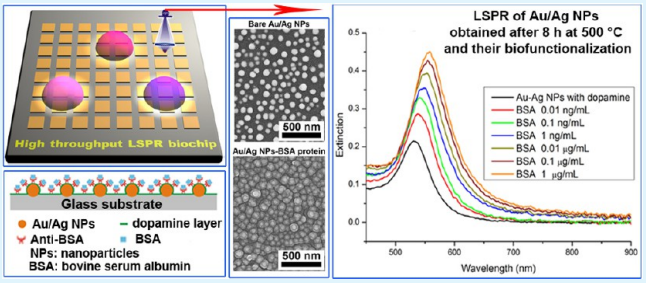

KEYWORDS: *gold/silver bimetallic nanoparticles, polydopamine surface functionalization, improved LSPR sensitivity, albumin detection*

INTRODUCTION

The last decades have witnessed the ongoing research interests in noble metal nanoparticles, especially for gold[1−5] and silver,[6−10] mainly due to their interesting optical properties. Specifically, the localized surface plasmonic resonance (LSPR) is derived from the inherent interaction between free electrons of a metal nanoparticle and incident electromagnetic wave,[11] which in turn leads to large optical absorption,[12] strong Rayleigh scattering,[13] and enhanced electronic field around the metal nanoparticles.[14,15] As a consequence, applications of noble metal nanoparticles have surged, including chemical and biochemical sensing,[16−19] medical diagnostics,[20] therapeutics,[21] waveguides,[22] optical devices,[23] and surface-enhanced spectroscopies.[24−26] By using nanoparticles with different compositions, sizes, and shapes,[27,28] the large plasmonic tunability from the visible to near-infrared spectral range can be realized. Specially, the nanostructures that have prominent plasmonic properties in the near-infrared spectrum are promising candidates for various nanomedicine applications, due to the weak absorption of biomaterials from the "biological window".[29] Besides the physical dimensions of nanoparticles, the plasmonic resonant peaks can also be affected by the localized dielectric environment surroundings which are explored as the basic mechanism for the emerging LSPR biosensors.[30]

In a typical LSPR biosensor configuration, the target analyte is recognized by the specific ligand modified on the surface of nanoparticles. This biochemical interaction leads to the increase of the refractive index of a local medium, transduced by plasmonic tuning of the resonant peak, including resonant wavelength shift and/or maximum optical density changes.[31,32] Such plasmonic characteristics are not only determined by the intrinsic refractive index sensitivity of metal nanoparticles but also dependent on the surface biofunctionalization of nanoparticles. For NPs of given size and shape, the intrinsic

Received: September 11, 2013
Accepted: November 26, 2013
Published: November 26, 2013

refractive index sensitivity is highly determined by the frequency-dependent dielectric function of materials. For instance, the silver nanoparticles (Ag NPs) have a larger magnitude of real part dielectric function when compared to gold nanoparticles, leading to more polarized charges in Ag NPs when excited by the incident light.[33] Since silver has a lower background polarizability of the d-band electrons, less plasmon damping effects are observed.[34] As a consequence, the Ag NPs have generally exhibited superior refractive index sensitivity (up to 2 times increase) when compared to that of Au NPs with the same geometric properties (size, shape, and aspect ratio).[35] However, the Ag NPs suffer from easy oxidation and potential toxicity. On the contrary, the Au NPs have good biocompatibility and excellent chemical stability, especially in the biological liquid phase. Moreover, due to the versatile reactivity of gold, plenty of chemical strategies can be employed to achieve the surface (bio)functionalization of gold nanoparticles,[36−38] which is advantageous for LSPR biosensing applications. To combine the advantages of silver (plasmonic sensitivity) and gold (chemical stability), there are many published articles focusing on the controlled preparation and study of the plasmonic properties of gold−silver alloy or bimetallic NPs.[39−43] In addition, the biocompatibility of these Au/Ag bimetallic NPs can be improved by surface modification of some biocompatible polymers like polydopamine.

Over the years, the nanoparticles used in plasmonic research have been prepared either by the "top-down" physical methods or the "bottom-up" chemical recipes where the uniform size and shape distribution, chemical composition, dispersion ability, and stability are the important parameters that need to be optimized.[44] Among these tremendous methodologies, the vacuum evaporation of gold thin film on glass substrate annealed at high temperature is considered as a facile and cost-effective way to obtain tunable gold plasmonic nanostructures.[45−48] However, the Au NPs obtained from the evaporation/annealing protocol suffered from multiple nanoparticle shapes, leading to an inhomogeneous broadening of the plasmon resonance peak.[49] The major disadvantage of prepared annealed Au NPs stems from their partial embedding inside the glass substrate, which obviously reduces the effective Au NP surface available for bimolecular functionalization. The prepared Au NPs with such a protocol show less plasmonic sensitivity.[50]

In this work, Au/Ag bimetallic NPs with homogeneous spherical shapes are obtained by evaporation through a TEM copper grid of silver (2 nm) onto the gold (4 nm) modified glass once exposed at high-temperature annealing (500 °C) for 8 h. The TEM grid is used as a maker to fabricate the well-organized patterns which can be further used as a high-throughput LSPR biochip, as reported in our previous work.[51] For biological applications, a facile and robust surface modification method based on the spontaneous polymerization of dopamine in base solution is employed on the NPs/glass interface before anti-albumin IgG antibody immobilization.

EXPERIMENTAL SECTION

Materials. Dopamine hydrochloride (H8502), trizma hydrochloride (T5941), 11-mercaptoundecanoic acid (674427), *N*-(3-dimethylaminopropyl)-*N*′-ethylcarbodiimide hydrochloride (E6383), *N*-hydroxysuccinimide (130672), and bovine serum albumin (A1253) were purchased from Sigma-Aldrich (Schnelldorf, Germany). Ethanol (02860), acetone (414689), and sodium hydroxide (S8045) were acquired from Fluka (Lyon, France). Phosphate buffer saline (PBS buffer, pH 7.4) was prepared using sodium chloride (S7653), sodium phosphate dibasic (94046), and sodium phosphate monobasic (71505) received from Sigma (St. Quentin Fallavier, France). Deionized water was produced by a Millipore water purification system (Molsheim, France). Monoclonal anti-BSA IgG antibody produced in mouse (B2901) was obtained from Sigma (Munich, Germany). BSA and anti-BSA IgG dilutions were prepared using PBS buffer. Classical glass microscope slides from Carl Roth GmbH (Germany) were used as the substrates, while commercial transmission electron microscope (TEM) copper grids (diameter of 3.05 mm, 200 meshes) were obtained from TED Pella (US).

Instruments. The optical microscope (Nikon, Eclipse LV100) and the field emission scanning electron microscope (Raith, FEG eLine) were used for substrate characterization of obtained micro/nanoplasmonic structures. A home-built confocal extinction measurement system was used to record the LSPR spectra from different zones of biochips in the UV−vis−NIR range from 200 to 1100 nm. The *LSPR optical setup* contained a white light source, two optical fibers (one for illumination and the other for collection), and an adjustable sample holder. It should be noted that due to the optical fibers and lens combinations used in the confocal setup, the incident beam with a spatial resolution of 10 μm was focused perpendicularly onto the patterned glass during all the measurements.

X-ray diffraction (XRD) measurements were conducted with a Seifert PTS-3000 X-ray diffractometer using Bragg−Brentano (θ−2θ) configuration and Cu Kα radiation and equipped with a Position Sensitive Detector. The XRD patterns were recorded for the 2θ angle range from 30° to 70° for all the measurements with a step size of 0.05°. To analyze the preferred orientation of the crystallites, the patterns were recorded for various inclination (tilt) angles χ from 0 to 65° with a step size of 5°.

Energy dispersive X-ray spectroscopy (EDS) measurements were performed on a field emission scanning electron microscope (FE-SEM, Hitachi SU8030) equipped with a Thermo Scientific Ultradry X-ray detector, and a thin layer (10 nm) of aluminum was deposited onto the sample surface to suppress the charging effects. The EDS spectra were recorded and analyzed using the Noran system7 software from Thermo Fisher Scientific. The acceleration voltage and working distance were 6 kV and 15 mm, respectively.

X-ray photoelectron spectroscopy (XPS) measurements were performed at room temperature on an Axis Nova instrument from a Kratos Analytical spectrometer with a monochromatic Al Kα line (1486.6 eV) source operated at 300 W. Survey spectra were acquired at pass energies of 80 eV. The core level spectra (C 1s, Au 4f, and Ag 3d) were acquired with an energy step of 0.1 eV and using a constant pass energy mode of 20 eV, to obtain data in a reasonable experimental time (energy resolution of 0.48 eV). XPS data were acquired for a minimum of three areas per sample. Data analysis was performed using CasaXPS software.

Preparation of Au/Ag Bimetallic NPs. Microscope glass slides were cut into small pieces (10 mm × 5 mm)^2 and used as substrates. Prior to metal evaporation, the glass substrates were washed with a mixture of detergent (Decon 90) and ddH_2O (1:9 volume ratio) in an ultrasonic water bath at 50 °C for 20 min and then dried within a N_2-stream. A commercial TEM copper grid was carefully fixed on top of the glass substrate as a mask. The metal evaporation was conducted in a vacuum evaporator (Plassys MEB400, France) using the electron beam mode with an evaporation rate of 0.05 nm/s monitored using a build-in quartz crystal sensor. The working pressure was 1.0×10^{-6} Torr. One gold layer (4 nm) followed by another silver layer (2 nm) were successively evaporated on the glass substrate through the TEM grid mask, and this is the optimized combination for biosensor application as discussed below. Moreover, other configurations with equivalent thicknesses (such as Au 4 nm, Au 6 nm, Ag 4 nm, Ag 6 nm, and Ag 2 nm followed by Au 4 nm and Ag 4 nm followed by Au 2 nm) were prepared as well. After the evaporation step, the grid mask was carefully removed, and the metal modified glass substrates were transferred into a high-temperature oven (Nabertherm, Germany) to be annealed at 500 °C for 8 h.

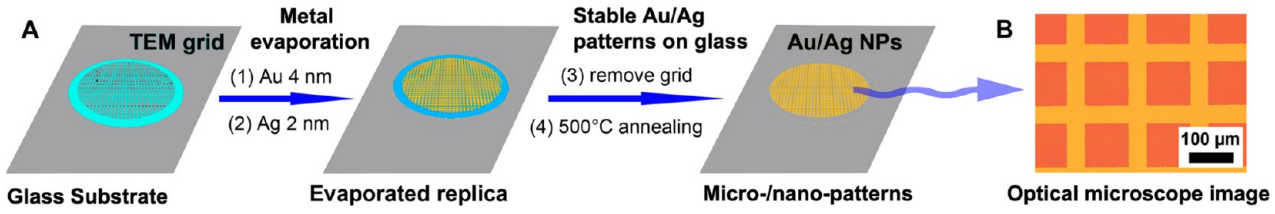

Figure 1. Fabrication steps of Au/Ag bimetallic NPs (A) and an optical microscope image of a gold TEM grid patterned onto the glass substrate (B). The orange squares contain Au/Ag bimetallic NPs.

Biofunctionalization of Au NPs and Au/Ag Bimetallic NPs. The annealed glass samples are first washed with an ethanol/acetone mixture solvent (1:1 volume ratio) in an ultrasonic water bath for 20 min at room temperature, followed by washing with ethanol and drying under N_2 stream. The resulted clean samples are vertically placed into a centrifuge tube containing 1 mL of dopamine solution (10 mM, pH = 8) in Tris-HCl buffer at room temperature for 1 h. Further, the dopamine-modified substrate is immersed in 1 mL of 11-mercapto-undecanoic acid (MUA) ethanolic solution (1 mM) for 12 h at room temperature, followed by washing with ethanol and drying under N_2 stream. The carboxylic group of the thiolated surface is activated with a mixture of EDC/NHS aqueous solution (0.4 mM/0.1 mM) at room temperature for 50 min. After aqueous washing and drying, 50 μL of anti-BSA IgG antibody diluted in PBS (0.1 mg/mL) is deposited onto the metal patterns for 5 h at 4 °C. After washing with PBS buffer and rinsing with ddH_2O, the antibody-modified substrate is used as a biochip for BSA protein detection. Specifically, 0.3 μL of different BSA concentrations (from 0.01 ng/mL to 10 μg/mL) are deposited onto different zones of glass micropatterned biochips. To complete the antibody−antigen interactions, albumin is incubated at 4 °C for 3 h. The plasmonic spectra corresponding to each biofunctionalization step are recorded by using extinction measurements. The control experiments are also conducted by immobilization of a BSA nonspecific antibody (anti-human IgG) on the biochip and exposed to the same concentrations of BSA. Since the spatial resolution of the test beam is 10 μm and one single patterned square of biochip is around 100 μm, five different areas within the same pattern are LSPR investigated. The obtained spectra are averaged in the final LSPR spectra to ensure the reproducibility.

RESULTS AND DISCUSSION

Preparation of Au/Ag Bimetallic NPs. Thanks to the commercial TEM copper grid used as a mask during the evaporation process, extremely well-organized and large-scale micropatterns of Au/Ag bimetallic NPs were developed after 8 h at 500 °C (Figure 1A). From the optical microscope image shown in Figure 1B, the gold/silver patterns were obtained after the careful removal of the TEM grid mask and sample annealing. One square of pattern measures (91 μm × 91 μm)^2, which is very close to the mesh size of the copper grid (90 μm × 90 μm)^2.

On the basis of the previous results,[49] the LSPR property evolutions of monometallic Au NPs are mainly determined by the gold evaporation thickness before annealing. Since the plasmon resonant wavelength is always red-shifted and broadens with the increase of gold evaporation thickness, the well-known interparticle coupling effects resulted from the Bragg diffraction of ordered arrays of metal nanostructures[52] are not observed in herein reported experiments, which could be attributed to the random distribution of obtained metallic NPs. In addition, the optimized monometallic Au NPs for biosensor applications correspond to a gold evaporation thickness of 4−6 nm.[47] Herein, the authors have chosen to further enhance the plasmonic sensitivity by incorporating silver into the previously optimized monometallic Au NPs with gold evaporation thickness of 4 nm.

Plasmonic and SEM Characterization of Nanoparticles. It has been reported that the plasmonic responses of silver nanoparticles are more sensitive than those of gold nanoparticles with the same geometrical properties.[35,53] It is well-known that bimetallic materials combined desirable properties that are not possessed by a single component (metal) alone.[54] The LSPR spectra of Au NPs and Au/Ag bimetallic NPs are investigated. Thus, a wider plasmonic peak is observed at 572 nm with a maximum optical density value of 0.29 for Au NPs (Figure 2A). After evaporation of silver (2 nm) onto a gold (4 nm) modified glass and annealing at 500 °C, a sharper plasmonic peak is recorded at 529 nm with an optical density value of 0.23 for Au/Ag bimetallic NPs. However, the samples with evaporated silver alone (4 or 6 nm) are not stable after annealing at 500 °C for 8 h, and the substrates become transparent without any LSPR peak recorded in the UV−NIR wavelength (see Figure S1 in the Supporting Information). Moreover the samples with first evaporation of Ag (4 nm) followed by Au evaporation (2 nm) or samples with Ag (2 nm) and Au (4 nm) show less intense plasmonic peaks (Figure S2A, B, Supporting Information) that lower the signal-to-noise ratio for biosensing applications. On the basis of the obtained results, the optimized bimetallic configuration is considered as Au (4 nm) followed by Ag (2 nm) evaporation. Moreover, the high sensitive plasmonic material (Ag) is the top layer in the optimized biosensor configuration, which can directly contribute to an improved LSPR sensitivity.

The SEM images of Au NPs and Au/Ag bimetallic NPs are illustrated in Figure 2B and 2C, respectively. The nanoparticle size distribution is obtained by using the public software ImageJ developed at the National Institutes of Health. Although extremely well-dispersed nanoparticles are obtained in both cases, the Au/Ag bimetallic NPs exhibited more uniform size and shape distribution when compared to Au NPs. Specifically, spherical and rod-like Au NPs with average size of 23.1 nm (Figure S3, Supporting Information) coexist, while dominant spherical Au/Ag NPs with average size of 36.6 nm (Figure S5, Supporting Information) annealed at the same temperature are identified. In addition, the average interparticle distance is larger in the case of Au/Ag bimetallic NPs. In the case of the 6 nm Au film, the NPs exhibit low frequency (25×) of 60 nm in diameter (Figure S4, Supporting Information).

On the basis of the morphological information of nanoparticles, the sharper plasmonic peak observed for Au/Ag bimetallic NPs could be attributed to more homogeneous spherical nanoparticles which significantly reduces the inhomogeneous broadening effects compared to Au NPs. Moreover, the blue-shift of the plasmon peak for Au/Ag bimetallic NPs could be attributed to the presence of a silver component.[3,34,53] In terms of plasmonic peak intensity, the

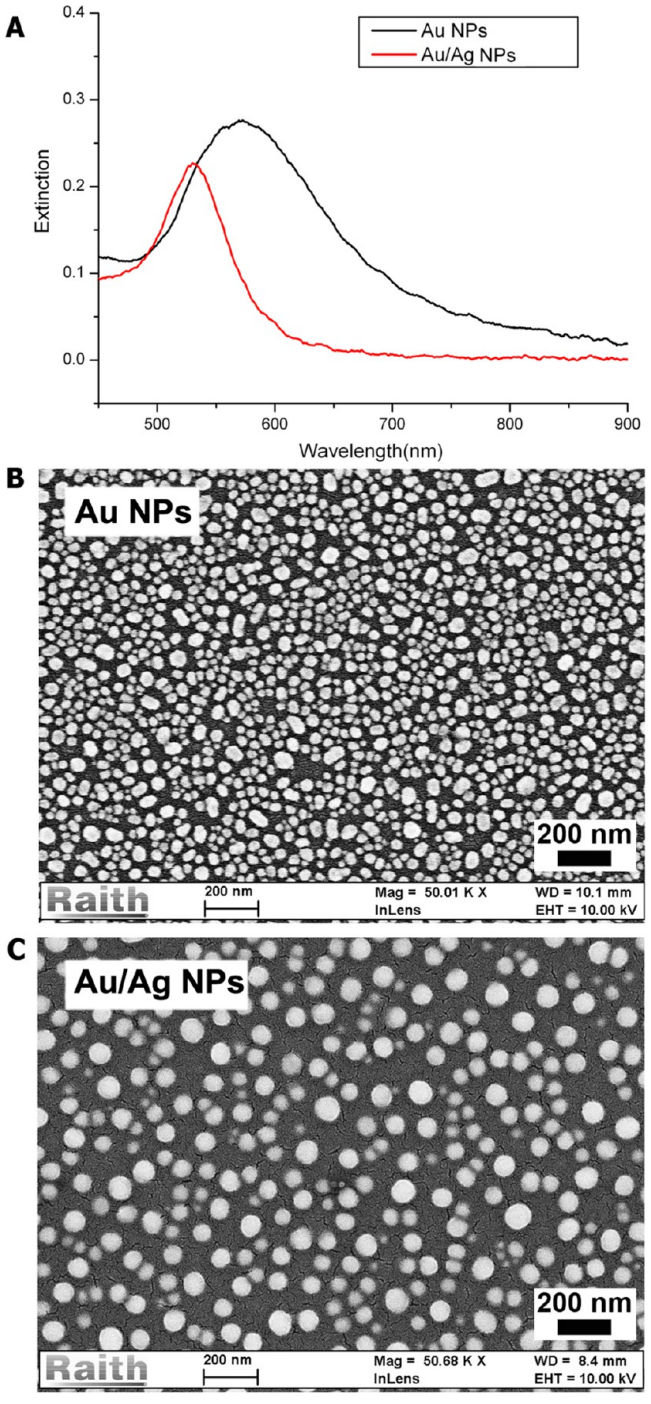

Figure 2. LSPR spectra (A) and SEM images of Au NPs (4 nm) (B) and Au (4 nm)/Ag (2 nm) bimetallic NPs (C). (Au – gold; Ag – silver).

authors believe that the presence of silver could also reduce the peak width. It should be noted that all the nanoparticles are fabricated by thermal annealing in the air atmosphere in this study, as the presence of oxygen is essential for the transformation of evaporated continuous film to isolated nanostructures on a glass substrate.[55]

LSPR Spectra Stability over Time. It should be noted that the 500 °C annealed Au/Ag bimetallic NPs are quite stable and resistant to oxidation, as the plasmonic spectra were almost constant for one week (see Figure S6A in Supporting Information), and the average value of resonant wavelength and maximum optical density (OD) from 6 days measurement is 530.6 ± 0.65 nm and 0.22 ± 0.008, respectively. On the contrary, the LSPR spectra for the Au 4 nm/Ag 2 nm sample annealed at 200 °C show obvious variations after three days storage (Figure S6B, Supporting Information). It is worth mentioning that all the bimetallic Ag/Au NPs are subjected to intensive ethanol and ddH_2O washing before LSPR measurement, which are the necessary steps used in biosensor experiments.

Nanostructured Surface Characterization Using XRD, EDS, and XPS. The X-ray diffraction patterns of Au 4 nm, Ag 2 nm, and Au 4 nm/Ag 2 nm samples were acquired before and after annealing, and the results are shown in Figure 3. For the

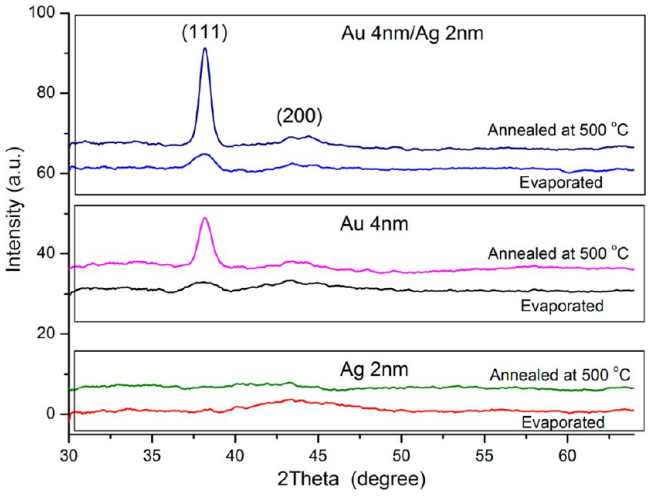

Figure 3. XRD patterns of gold (Au 4 nm), silver (Ag 2 nm), and gold–silver (Au 4 nm/Ag 2 nm) samples before and after annealing at 500 °C for 8 h.

deposited metal before annealing, the diffraction peak (111) of gold or silver is weak and very broad, indicating that the evaporated gold or silver thin film on glass is not well crystallized. Remarkably, the XRD patterns were significantly changed after annealing at 500 °C for 8 h. The samples of monometallic Au NPs and bimetallic Au/Ag NPs show diffraction peaks of gold or silver (please note that gold and silver have a similar lattice parameter), respectively, and (111) and (200) planes at $2\theta = 38.2°$ and 44.4° (JCPDS cards no. 04-0784 for Au and no. 04-0783 for Ag). It should be noted that although the silver seems not stable after annealing, the combination of gold and silver leads to the sharpest peak of highest intensity corresponding to the (111) plane, indicating that the crystallinity degree of Au/Ag bimetallic NPs is higher than that of Au monometallic NPs. For both Au NPs and Au/Ag NPs, it was found that the intensity of (111) reflection decreases steadily when the tilt angle goes from 0 to 65°, indicating that the crystallites are oriented with (111) planes parallel to the surface of the substrate.

The EDS technique was used to verify the presence of silver in the Au 4 nm/Ag 2 nm bimetallic systems. Different areas of the sample before and after annealing were imaged using FE-SEM (see Figure S7 in Supporting Information) and then were analyzed by the EDS technique to quantify the atomic composition of the bimetallic sample. It is found that the silver atomic weight percentage is 22.0% for the evaporated sample (Figure 4A), which is very close to the calculated silver percentage of 21.5%. After annealing, the silver atomic

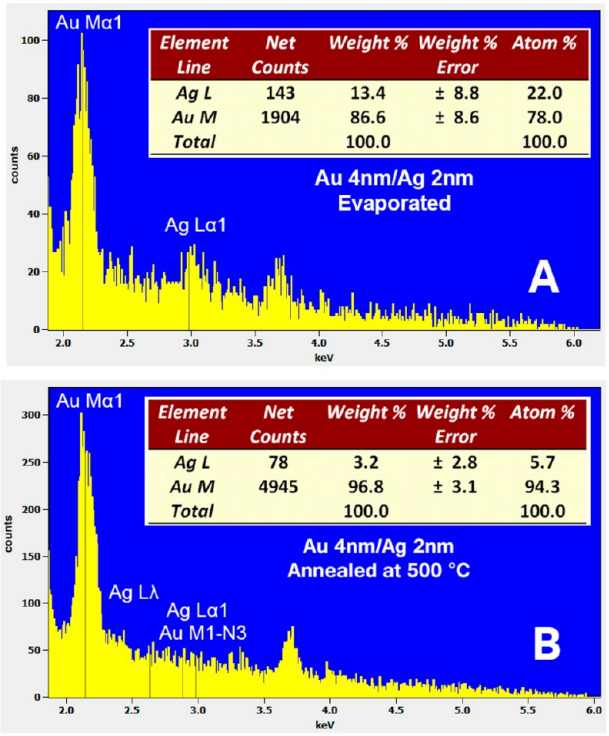

Figure 4. Energy-dispersive X-ray spectrum of the Au 4 nm/Ag 2 nm sample before annealing (A) and after annealing at 500 °C for 8 h (B). The element composition tables shown in the inset were obtained by the software Noran system7.

percentage is obviously decreased to 5.7% (Figure 4B), which confirms the possible evaporation loss of silver during high-temperature annealing. The noises in the EDS spectrum are due to the fact that the thickness of the glass substrate is much larger than the size of the Au/Ag nanoparticles.

The XPS spectra of three annealed samples of monometallic Au NPs, Ag NPs, and bimetallic Au/Ag NPs were shown in Figure 5, concerning the calibration, and the binding energy for the C 1s hydrocarbon peak was set at 284.8 eV (see Figure S8 in the Supporting Information). For the annealed monometallic Au NPs, two typical peaks were obtained at 83.6 and 87.3 eV, respectively, corresponding to the $4f_{7/2}$ and $4f_{5/2}$ peaks of gold (Figure 5A), while for the bimetallic Au/Ag NPs, these two peaks were slightly shifted to the higher energy at 84.0 and 87.7 eV, respectively. For the Ag XPS spectra shown in Figure 5B, there are no silver signatures detected for the monometallic Ag NPs. Interestingly, the two peaks of Ag $3d_{5/2}$ and Ag $3d_{3/2}$ at 367.9 and 373.8 eV, respectively, were obtained for bimetallic Au/Ag NPs, indicating that the possible silver evaporation can be avoided in the bimetallic NPs system.

It should be emphasized that the plasmonic resonant wavelength of bimetallic Au/Ag NPs is independent of evaporation order of gold and silver before annealing; therefore, the bimetallic nanoparticles behave like gold/silver alloys. Such results can explain the remarkable LSPR stability over time after intensive aqueous washing steps (Figure S6, Supporting Information), which ensure their application in the following biosensor section. Moreover, due to the high annealing temperature, there are no obvious signals detected for the monometallic Ag sample from LSPR (Figure S1, Supporting Information), XRD (Figure 3), and XPS (Figure 5) measurements, while the exact reason for the "disappearance" of silver

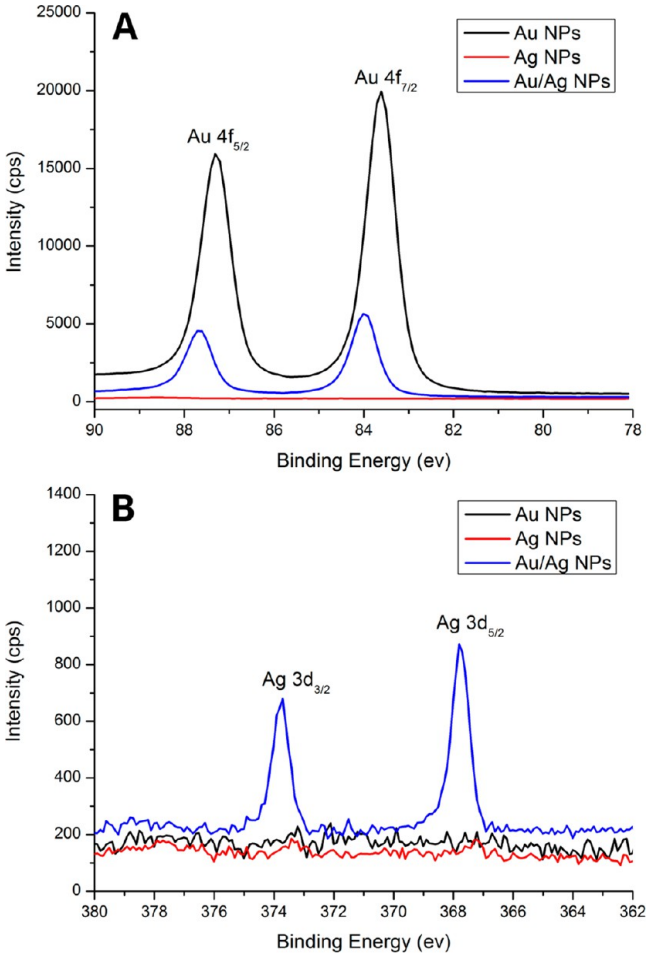

Figure 5. XPS spectra for (A) Au 4f and (B) Ag 3d for the monometallic Au NPs, Ag NPs, and bimetallic Au/Ag NPs.

after annealing remains unclear and more experiments will be conducted in the near future.

Enhanced Plasmonic Behavior of Au/Ag Bimetallic NPs. Inspired from the mussel's strong adhesive ability to almost any type of organic and inorganic surfaces, a quite cost-effective, very efficient, and robust surface modification protocol, based on the spontaneous polymerization of the chemical compound dopamine in base solution, has been developed by Phillip B. Messersmith and co-workers.[56] It has been found that a thin film of polydopamine can be deposited on almost any surface just by dipping the sample into a base solution of dopamine. More interestingly, the thickness of the resulted polymer film could be adjusted easily by controlling the dipping time.[56,57] Since the plasmonic properties of noble metal nanoparticles show strong distance dependence (the characteristic decay length up to a few tens of nanometers is reported), the dopamine-based surface modification protocol is applied for the first time for Au and Au/Ag bimetallic NPs.

For biological diagnostics for annealed Au and Au/Ag using plasmonic sensitivity, the Au and Au/Ag bimetallic NP samples are immersed in 10 mM dopamine solution (1 mL) of Tri-HCl buffer (pH = 8.5) for different periods of time (Figure S9, Supporting Information). It is noticed that with the increasing of the reaction time the steady red-shift of resonant wavelength and the maximum peak intensity are recorded for both Au NPs and Au/Ag bimetallic NPs. Variation of the resonant wavelength length, the maximum OD, full width at half-

dx.doi.org/10.1021/am403943q | ACS Appl. Mater. Interfaces 2014, 6, 219−227

maximum (fwhm), Q factor, and modified figure of merit (FoM) values as a function of the dopamine incubation time are reported in Table 1. Thus, in the case of Au NPs, after 6 h

Table 1. LSPR Analytical Performances of Au NPs and Au/Ag Bimetallic NPs Independently Exposed to Dopamine Solution (1 mM) for Different Periods of Time at Room Temperature

	sample	0 h	1 h	2 h	4 h	6 h
Au NPs	wavelength (nm)	551.6	561.7	569.4	573.3	581.1
	optical density (OD)	0.21	0.22	0.25	0.28	0.3
	fwhm (nm)	82.1	91.3	97.4	104.2	111.1
	Q factor[a]	6.72	6.15	5.85	5.5	5.23
	figure of merit (FoM)[b]	---	0.11	0.18	0.21	0.27
Au/Ag NPs	wavelength (nm)	529.1	535.3	538.4	544.7	556.3
	optical density (OD)	0.23	0.27	0.3	0.35	0.4
	fwhm (nm)	45.9	51.3	53.6	59.7	62.1
	Q factor	11.54	10.45	10.05	9.12	8.98
	figure of merit (FoM)	---	0.12	0.19	0.26	0.45

[a]Q factor = λ_{max}/fwhm, λ_{max} is the maximum resonant wavelength. [b]Figure of merit (FoM) = $\Delta\lambda_{max}$/fwhm, and $\Delta\lambda_{max}$ is the shift of maximum resonant wavelength using the resonant wavelength at 0 h coating time as the references (551.6 nm for Au NPs and 529.1 nm for Au/Ag bimetallic NPs).

treatments with dopamine, a 30 nm red-shift of resonant wavelength and 0.09 increase of maximum OD value are noticed. Interestingly, for the Au/Ag bimetallic NPs, although presenting a similar red-shift of wavelength (29 nm), a much larger maximum OD value increase of 0.17 is obtained, which is almost twice enhanced when compared to Au NPs.

On the basis of the above-reported results, the authors unambiguously demonstrated that plasmonic sensitivity of Au/Ag bimetallic NPs is clearly enhanced when compared to Au NPs, especially for the increase of maximum optical density upon different types of biofunctionalization of bimetallic particles. Although the exact mechanisms responsible for the improvement of plasmonic responses in the presence of dopamine are yet to be explored, the introduction of more sensitive plasmonic material such as silver in the fabrication of bimetallic materials could normally induce better LSPR properties than those of a single metal.[53]

High-Throughput LSPR Detection of BSA Using (Bio)functionalized Bimetallic NPs. Since the Au/Ag bimetallic NPs have exhibited more sensitive plasmonic responses than Au NPs, they can be used as substrates for the construction of immunosensors for sensitive detection of albumin. Due to the TEM grid mask, the large scale (in millimeter range) of micro/nanoplasmonic structures is easily prepared. In addition, the incident beam can be launched precisely to different zones of NPs with the spatial resolution of 10 μm assured by the home-built confocal measurement setup. The easily addressed micropatterns on glass enable the same NP zones to be tested after each biosensor preparation step, which obviously improves the measurement reproducibility. Therefore, the resulted well-organized micro/nanostructures are used as high-throughput biochips to sequentially detect several chemical compounds. Experimentally, different concentrations of BSA antigen (0.3 μL) are deposited onto the different areas of the antibody-modified NP biochips. One biochip contains one TEM grid patterned area for the detection of three different concentrations of BSA antigen. The plasmonic responses corresponding to different concentrations of BSA ranging from 0.01 ng/mL to 10 μg/mL are shown in Figure 6.

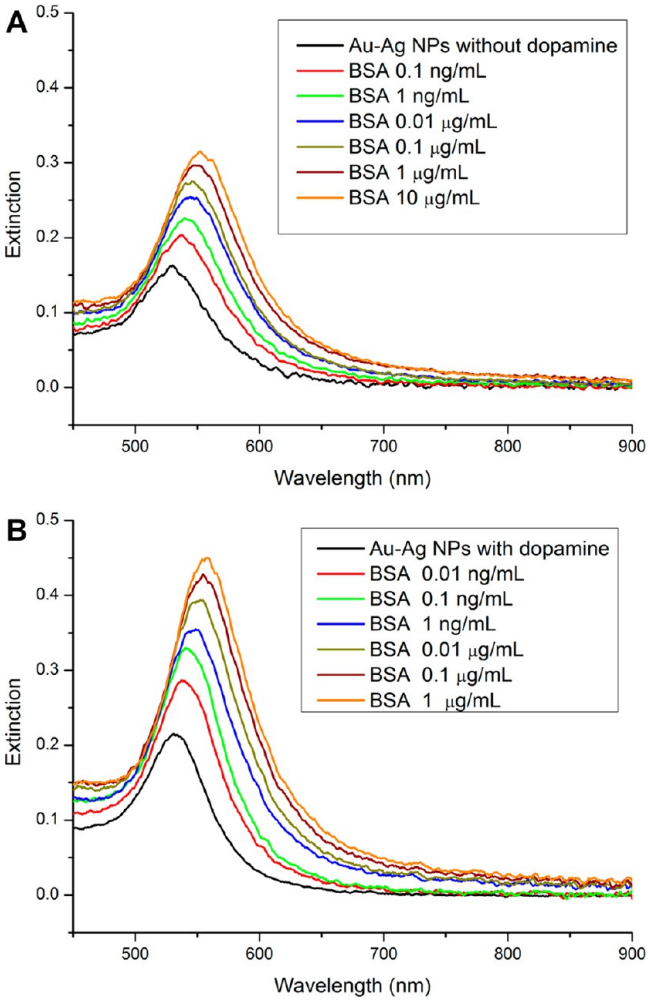

Figure 6. LSPR spectra of Au/Ag bimetallic NPs without (A) and with (B) dopamine film (coating time is 1 h) to detect different BSA concentrations starting from 0.01 ng/mL up to 10 μg/mL. For each TEM grid patterned chip, up to three drops of different BSA concentrations are deposited using a micropipet for LSPR detection.

It is found that the LSPR biosensor based on Au–Ag bimetallic NPs are able to discriminate different concentrations of BSA antigen (see Figure 6A). Specifically, as the BSA concentration increases from 0.1 ng/mL to 10 μg/mL, a red-shift of resonant wavelength (from 535.9 to 554.6 nm) and an increase of OD (from 0.2 to 0.32) were observed, respectively.

Experimentally it was found that the annealed Au/Ag bimetallic NPs are quite stable in the liquid phase during extensive biofunctionalization steps, mainly due to their partial embedding inside the glass after 8 h at 500 °C. However, the effective surface area of metal nanoparticles is expected to

decline, affecting the binding quantity of the antibody molecule, which finally may result in a less sensitive response to antigen molecule recognition.[46,50]

To further increase the plasmonic sensitivity of high-temperature annealed NPs on the glass substrate, the dopamine surface modification is used in this work. Since the spontaneous dopamine polymerization protocol in base solution can occur at almost any surface, it is expected that both the Au/Ag bimetallic NPs and the interstitial spaces between NPs can be modified with a uniform layer of polydopamine. Even more interestingly, the dopamine-modified surface can be used to bind thiol via the Michael addition between catechol and thiol groups.[57,58] Since the localized surface plasmon resonance is rapidly damping away from nanoparticles, the thickness of the polydopamine layer should be carefully controlled to make sure that the biomolecule binding is in the plasmonic sensing volume. Therefore, the annealed Au/Ag bimetallic NPs subject to 1 h dopamine treatment prior to thiol modification are used to improve the LSPR sensitivity. Moreover, the surface modification with polydopamine also improves the biocompatibility and oxidation resistance of the top silver layer for the obtained Au−Ag bimetallic NPs.

Indeed, from the plasmonic spectra recorded from Ag/Au bimetallic NPs modified with dopamine (Figure 6B), a larger shift of resonant wavelength and increase of optical density are recorded when exposed to the BSA antigen. Specifically, a plasmonic peak red-shifted from 536.9 to 561.4 nm and a larger OD increase of 0.17 are obtained upon specific binding of different BSA concentrations from 0.01 ng/mL to 1 μg/mL. The plasmonic responses are saturated for the higher BSA concentration (10 μg/mL). The control experiment using the same Au−Ag-dopamine NPs modified with a BSA nonspecific antibody was also conducted, where the different concentrations of BSA cannot be detected (Figure S10, Supporting Information). These results confirm that the specific plasmonic changes reported in Figure 6B result from specific antibody−antigen interaction.

The calibration curves for detection of different concentrations of BSA using Au−Ag bimetallic NPs without and with dopamine modification are depicted in Figure 7. Moreover, the results from the monometallic Au NPs are included as well. In terms of the lower limit of detection, 1 ng/mL of BSA is detectable using monometallic naked Au NPs, while the lower concentration of 0.1 ng/mL BSA can be readily determined by using Au−Ag bimetallic NPs. The sensitivity is further increased to 0.01 ng/mL for Au−Ag bimetallic NPs modified with polydopamine, which is lower than the analytical sensitivity (0.5 ng/mL) of a recently published BSA biosensor study.[59] Moreover, a much larger linear detection range of 0.01−100 ng/mL is obtained under the optimized conditions.

Since the plasmonic responses are saturated at the highest BSA concentration of 10 μg/mL, the surface morphology of Au/Ag bimetallic NPs modified with this concentration of BSA is characterized with scanning electron microscopy (SEM). For the Au/Ag bimetallic NPs without dopamine treatment (Figure 8A), a rough surface morphology is observed as albumin aggregates are formed, indicating a successful biofunctionalization step. Interestingly, the BSA coating layer is mainly found around or near the metal nanoparticles, while for the interstitial spaces between NPs no obvious protein depositions are observed. However, for the Au/Ag bimetallic NPs with dopamine treatment (Figure 8B), the entire sample surface was modified with albumin molecules. Moreover, structures like

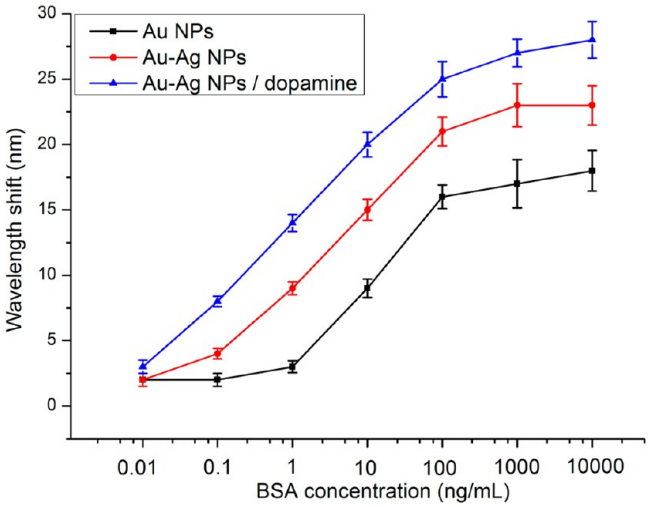

Figure 7. Calibration curves for BSA detection using different substrates of monometallic Au NPs (black curve), bimetallic Au−Ag NPs (red curve), and dopamine-modified Au−Ag bimetallic NPs (blue curve). The evaporation thicknesses of Au and Ag are 4 and 2 nm, respectively. All samples were annealed at 500 °C for 8 h. Three experiments were conducted for each substrate, and the average results are shown in the above figure.

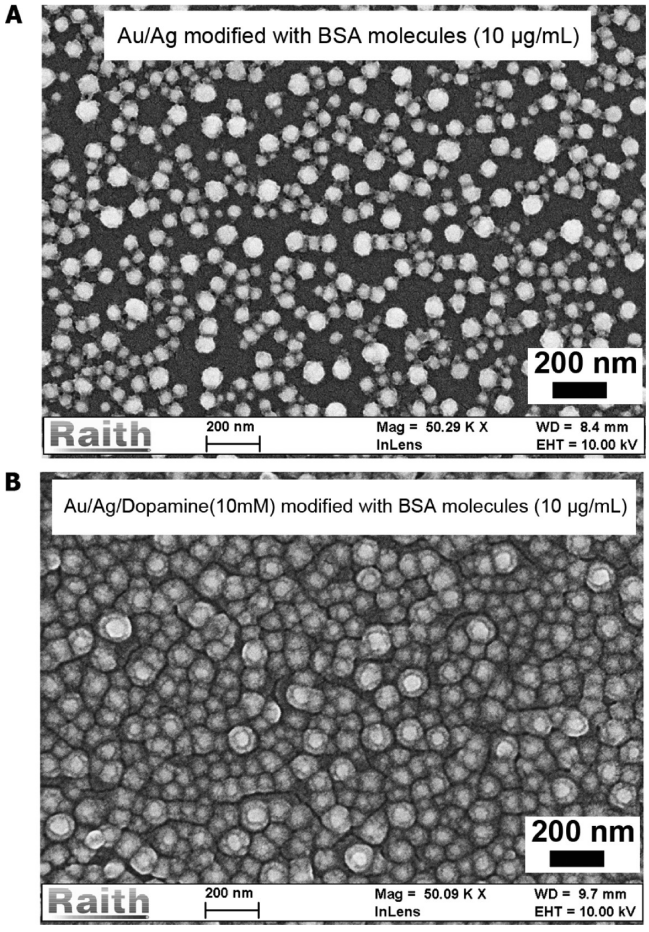

Figure 8. SEM images of Au/Ag bimetallic NPs without (A) and with (B) dopamine treatment after BSA antigen (10 μg/mL) immunoreactions with anti-BSA antibody (0.1 mg/mL).

"core−shell" are clearly visible for bigger NPs on the glass substrate (Figure 8B).

dx.doi.org/10.1021/am403943q | ACS Appl. Mater. Interfaces 2014, 6, 219−227

Although it is difficult to probe the exact composition of glass surface modified with Au/Ag/dopamine/antibody/BSA antigen films, the authors emphasize that such NP functionalization steps are observed over several repeated experiments when the samples have been exhaustively rinsed with ddH_2O and ethanol to remove any possible impurities prior to the SEM imaging characterization. On the basis of the above surface treatment protocol, the observed SEM morphology could be attributed mainly to the specific presence of BSA molecules and polydopamine films.

CONCLUSIONS

In this work, extremely well-organized and stable Au/Ag bimetallic NPs are fabricated on glass after 8 h annealing at high temperature (500 °C). It was found that fabricated Au/Ag bimetallic NPs have a sharper plasmonic peak in the visible spectrum range with plasmonic responses more sensitive than those of Au NPs. To increase the sensitivity of the LSPR immunosensor, a surface modification strategy based on the multifunctional polydopamine layer coating Au/Ag bimetallic NPs is explored to increase the immobilization quantity of antibody. Thus, as low as 0.01 ng/mL of BSA can be detected under the optimized conditions. The proposed nanoparticle treatment contributes to the development of sensitive LSPR biochips that are able to detect different concentrations of protein in a simple and high-throughput manner.

ASSOCIATED CONTENT

Supporting Information

Figures S1−S10. This material is available free of charge via the Internet at http://pubs.acs.org.

AUTHOR INFORMATION

Corresponding Author

*E-mail: elena_rodica.ionescu@utt.fr. Fax: +(33) 3 25 71 84 56. Tel.: +(33) 3 25 75 97 28.

Notes

The authors declare no competing financial interest.

ACKNOWLEDGMENTS

The authors thank the Stratégique Program 2009−2012 financed by University of Technology of Troyes (UTT), the Region Champagne-Ardenne grant NANO'MAT for electron microscope characterization, and the ANR program ANR-07-Nano-032 "NP/CL" for supplement of the optical setup. Dr. Ionescu also thanks the OSEO Innovation Programme for supporting the projet "Système de procédé de détection d'espèces biologiques ou chimiques QCM structuré" 2012-2014. The authors thank Serguei Kochtcheev for his help on sample processing in EDS experiments, while K.J. and Y.L. kindly thank the Chinese Scholarship Council (CSC) for funding their PhD scholarship in France.

REFERENCES

(1) Grzelczak, M.; Perez-Juste, J.; Mulvaney, P.; Liz-Marzan, L. M. *Chem. Soc. Rev.* **2008**, *37*, 1783−1791.
(2) Daniel, M. C.; Astruc, D. *Chem. Rev.* **2004**, *104*, 293−346.
(3) Lee, S. Y.; Kim, S. H.; Jang, S. G.; Heo, C. J.; Shim, J. W.; Yang, S. M. *Anal. Chem.* **2011**, *83*, 9174−9180.
(4) Corbierre, M. K.; Beerens, J.; Beauvais, J.; Lennox, R. B. *Chem. Mater.* **2006**, *18*, 2628−2631.
(5) Vedantam, P.; Tzeng, T. R. J.; Brown, A. K.; Podila, R.; Rao, A.; Staley, K. *Plasmonics* **2012**, *7*, 301−308.
(6) Rycenga, M.; Cobley, C. M.; Zeng, J.; Li, W. Y.; Moran, C. H.; Zhang, Q.; Qin, D.; Xia, Y. N. *Chem. Rev.* **2011**, *111*, 3669−3712.
(7) Wang, H. H.; Liu, C. Y.; Wu, S. B.; Liu, N. W.; Peng, C. Y.; Chan, T. H.; Hsu, C. F.; Wang, J. K.; Wang, Y. L. *Adv. Mater.* **2006**, *18*, 491−495.
(8) Ren, X. L.; Meng, X. W.; Chen, D.; Tang, F. Q.; Jiao, J. *Biosens. Bioelectron.* **2005**, *21*, 433−437.
(9) Liu, C. H.; Li, Z. P.; Du, B. A.; Duan, X. R.; Wang, Y. C. *Anal. Chem.* **2006**, *78*, 3738−3744.
(10) Behrens, S.; Wu, J.; Habicht, W.; Unger, E. *Chem. Mater.* **2004**, *16*, 3085−3090.
(11) Willets, K. A.; Van Duyne, R. P. *Annu. Rev. Phys. Chem.* **2007**, *58*, 267−297.
(12) El-Sayed, M. A. *Acc. Chem. Res.* **2001**, *34*, 257−264.
(13) Michaels, A. M.; Nirmal, M.; Brus, L. E. *J. Am. Chem. Soc.* **1999**, *121*, 9932−9939.
(14) Kelly, K. L.; Coronado, E.; Zhao, L. L.; Schatz, G. C. *J. Phys. Chem. B* **2003**, *107*, 668−677.
(15) Smitha, S. L.; Gopchandran, K. G.; Ravindran, T. R.; Prasad, V. S. *Nanotechnology* **2011**, *22*, 265705.
(16) Mayer, K. M.; Hafner, J. H. *Chem. Rev.* **2011**, *111*, 3828−3857.
(17) Szunzerits, S.; Boukherroub, R. *Chem. Commun.* **2012**, *48*, 8999−9010.
(18) Yanik, A. A.; Cetin, A. E.; Huang, M.; Artar, A.; Mousavi, S. H.; Khanikaev, A.; Connor, J. H.; Shvets, G.; Altug, H. *Proc. Natl. Acad. Sci. U.S.A.* **2011**, *108*, 11784−11789.
(19) Choi, I.; Song, H. D.; Lee, S.; Yang, Y. I.; Kang, T.; Yi, J. *J. Am. Chem. Soc.* **2012**, *134*, 12083−12090.
(20) Dreaden, E. C.; Alkilany, A. M.; Huang, X. H.; Murphy, C. J.; El-Sayed, M. A. *Chem. Soc. Rev.* **2012**, *41*, 2740−2779.
(21) Huang, X. H.; El-Sayed, I. H.; Qian, W.; El-Sayed, M. A. *J. Am. Chem. Soc.* **2006**, *128*, 2115−2120.
(22) Oulton, R. F.; Sorger, V. J.; Genov, D. A.; Pile, D. F. P.; Zhang, X. *Nat. Photonics* **2008**, *2*, 496−500.
(23) Dragoman, M.; Dragoman, D. *Prog. Quantum Electron.* **2008**, *32*, 1−41.
(24) Kneipp, K.; Wang, Y.; Kneipp, H.; Perelman, L. T.; Itzkan, I.; Dasari, R. R.; Feld, M. S. *Phys. Rev. Lett.* **1997**, *78*, 1667−1670.
(25) Aslan, K.; Geddes, C. D. *Anal. Chem.* **2009**, *81*, 6913−6922.
(26) Halas, N. J.; Lal, S.; Chang, W. S.; Link, S.; Nordlander, P. *Chem. Rev.* **2011**, *111*, 3913−3961.
(27) Ringe, E.; McMahon, J. M.; Sohn, K.; Cobley, C.; Xia, Y. N.; Huang, J. X.; Schatz, G. C.; Marks, L. D.; Van Duyne, R. P. *J. Phys. Chem. C* **2010**, *114*, 12511−12516.
(28) Peng, S.; McMahon, J. M.; Schatz, G. C.; Gray, S. K.; Sun, Y. G. *Proc. Natl. Acad. Sci. U.S.A.* **2010**, *107*, 14530−14534.
(29) Jin, Y. D. *Adv. Mater.* **2012**, *24*, 5153−5165.
(30) Anker, J. N.; Hall, W. P.; Lyandres, O.; Shan, N. C.; Zhao, J.; Van Duyne, R. P. *Nat. Mater.* **2008**, *7*, 442−453.
(31) Zhao, J.; Zhang, X. Y.; Yonzon, C. R.; Haes, A. J.; Van Duyne, R. P. *Nanomedicine* **2006**, *1*, 219−228.
(32) Haes, A. J.; Van Duyne, R. P. *J. Am. Chem. Soc.* **2002**, *124*, 10569−10604.
(33) Lee, Y. H.; Chen, H. J.; Xu, Q. H.; Wang, J. F. *J. Phys. Chem. C* **2011**, *115*, 7997−8004.
(34) Lee, K. S.; El-Sayed, M. A. *J. Phys. Chem. B* **2006**, *110*, 19220−19225.
(35) Jakab, A.; Rosman, C.; Khalavka, Y.; Becker, J.; Trugler, A.; Hohenester, U.; Sonnichsen, C. *ACS Nano* **2011**, *5*, 6880−6885.
(36) Aslan, K.; Perez-Luna, V. *Langmuir* **2002**, *18*, 6059−6065.
(37) Tkachenko, A. G.; Xie, H.; Coleman, D.; Glomm, W.; Ryan, J.; Anderson, M. F.; Franzen, S.; Feldheim, D. L. *J. Am. Chem. Soc.* **2003**, *125*, 4700−4701.
(38) Hurst, S. J.; Lytton-Jean, A. K. R.; Mirkin, C. A. *Anal. Chem.* **2006**, *78*, 8313−8318.
(39) Imamova, S.; Nedyalkov, N.; Dikovska, A.; Atanasov, P.; Sawczak, M.; Jendrzejewski, R.; Sliwinski, G.; Obara, M. *Appl. Surf. Sci.* **2010**, *257*, 1075−1079.

(40) Sancho-Parramon, J.; Janicki, V.; Loncaric, M.; Zorc, H.; Dubcek, P.; Bernstorff, S. *Appl. Phys. A: Mater. Sci. Process.* **2011**, *103*, 745−748.
(41) Xu, L.; Tan, L. S.; Hong, M. H. *Appl. Opt.* **2011**, *50*, G74−G79.
(42) Wu, W.; Njoki, P. N.; Han, H.; Zhao, H.; Schiff, E. A.; Lutz, P. S.; Solomon, L.; Matthews, S.; Maye, M. M. *J. Phys. Chem. C* **2011**, *115*, 9933−9942.
(43) Qi, W. H.; Lee, S. T. *J. Phys. Chem. C* **2010**, *114*, 9580−9587.
(44) Jones, M. R.; Osberg, K. D.; Macfarlane, R. J.; Langille, M. R.; Mirkin, C. A. *Chem. Rev.* **2011**, *111*, 3736−3827.
(45) Karakouz, T.; Tesler, A. B.; Bendikov, T. A.; Vaskevich, A.; Rubinstein, I. *Adv. Mater.* **2008**, *20*, 3893−3899.
(46) Kedem, O.; Tesler, A. B.; Vaskevich, A.; Rubinstein, I. *ACS Nano* **2011**, *5*, 748−760.
(47) Jia, K.; Bijeon, J. L.; Adam, P. M.; Ionescu, R. E. *Anal. Chem.* **2012**, *84*, 8020−8027.
(48) Karakouz, T.; Maoz, B. M.; Lando, G.; Vaskevich, A.; Rubinstein, I. *ACS Appl. Mater. Interfaces* **2011**, *3*, 978−987.
(49) Jia, K.; Bijeon, J. L.; Adam, P. M.; Ionescu, R. E. *Plasmonics* **2013**, *8*, 143−151.
(50) Karakouz, T.; Holder, D.; Goomanovsky, M.; Vaskevich, A.; Rubinstein, I. *Chem. Mater.* **2009**, *21*, 5875−5885.
(51) Jia, K.; Bijeon, J. L.; Adam, P. M.; Ionescu, R. E. *Analyst* **2013**, *138*, 1015−1019.
(52) Kravets, V. G.; Schedin, F.; Grigorenko, A. N. *Phys. Rev. Lett.* **2008**, *101*, 087403.
(53) Jiang, R. B.; Chen, H. J.; Shao, L.; Li, Q.; Wang, J. F. *Adv. Mater.* **2012**, *24*, OP200−OP207.
(54) Cortie, M. B.; McDonagh, A. M. *Chem. Rev.* **2011**, *111*, 3713−3735.
(55) Yan, C.; Chen, Y.; Jin, A.; Wang, M.; Kong, X.; Zhang, X.; Ju, Y.; Han, L. *Appl. Surf. Sci.* **2011**, *258*, 377−381.
(56) Lee, H.; Dellatore, S. M.; Miller, W. M.; Messersmith, P. B. *Science* **2007**, *318*, 426−430.
(57) Kang, S. M.; Hwang, N. S.; Yeom, J.; Park, S. Y.; Messersmith, P. B.; Choi, I. S.; Langer, R.; Anderson, D. G.; Lee, H. *Adv. Funct. Mater.* **2012**, *22*, 2949−2955.
(58) Lee, Y.; Chung, H. J.; Yeo, S.; Ahn, C. H.; Lee, H.; Messersmith, P. B.; Park, T. G. *Soft Matter* **2010**, *6*, 977−983.
(59) Zhang, M.; Yan, M.; Yu, J. H.; Ge, S. G.; Wan, F. W.; Ge, L. *Anal. Methods* **2012**, *4*, 460−466.